Revised magnetostratigraphy and characteristics of the fluviolacustrine sedimentation of the Kashmir basin, India, during Pliocene-Pleistocene

N. Basavaiah,[1] E. Appel,[2] B. V. Lakshmi,[1] K. Deenadayalan,[1] K. V. V. Satyanarayana,[1] Saumitra Misra,[1] N. Juyal,[3] and M. A. Malik[4]

Received 6 August 2009; revised 30 March 2010; accepted 19 April 2010; published 24 August 2010.

[1] The Pliocene-Pleistocene Karewa Group sediments of the Kashmir basin, India, provide an important continental archive for past climatic reconstruction. The present study reevaluates the magnetic polarity stratigraphy and the nature of the depositional environment at a 440-m-thick section along Romushi river near Pakharpur (33°48′50″N, 74°45′54″E). Magnetic remanences are predominantly carried by Ti-rich titanomagnetite and magnetite. We identified eight normal and eight reversed-polarity magnetozones in this succession, ranging between 4.40 and 0.77 Ma. The polarity sequence includes the new identification of the Cochiti and the Mammoth and their preceding and succeeding reversed/normal as well as the Jaramillo subchrons. Anisotropy of magnetic susceptibility data suggest the existence of northeast- and northwest-flowing fluvial system before 4.18 Ma, indicating the Pir Panjal range at the southwest as the sediment source area. Following this, the valley was under the influence of fluviolacustrine environment between 4.18 and 0.77 Ma. Our results suggest relatively strong flow velocity toward the northeast during the upper Gilbert, Gauss, and lower and middle Matuyama chrons (4.18–1.07 Ma). In the upper Matuyama chron (<1.07 Ma), the prevailing paleocurrent direction in the basin changed toward the northwest with a reduced flow velocity, indicating the emergence of the ancestral Jhelum river. On the basis of the magnetic polarity chronology, the sediment accumulation rate indicates a very low value of ~4.6 cm kyr^{-1} before 1.95 Ma to ~33 cm kyr^{-1} between 1.95 and 1.77 Ma and 23 cm kyr^{-1} after 1.77 Ma. We attribute temporal changes in sedimentation rate to the interplay between climate (predominantly westerlies) and tectonics (pulsating Pir Panjal uplift).

Citation: Basavaiah, N., E. Appel, B. V. Lakshmi, K. Deenadayalan, K. V. V. Satyanarayana, S. Misra, N. Juyal, and M. A. Malik (2010), Revised magnetostratigraphy and characteristics of the fluviolacustrine sedimentation of the Kashmir basin, India, during Pliocene-Pleistocene, *J. Geophys. Res.*, *115*, B08105, doi:10.1029/2009JB006858.

1. Introduction

[2] The Kashmir valley is an intermontane basin within the Himalayan mountain ranges. It is located north of the main boundary thrust and south of the Great Himalaya range, between the northwest-to-southeast trending Panjal thrust in the southwest and the subparallel Zanskar thrust in the northeast (*Agarwal and Agrawal* [2005] and references therein) (Figure 1a). Other, similar large intermontane basins along the southern Tibetan plateau margin are the Kathmandu basin, Nepal, in the central Himalayas [*Yoshida and Igarashi*, 1984], and the Heqing basin, Yunnan Province, China, at the southeastern margin of the plateau [*Yang et al.*, 2000]. These basins generally represent "extensional rift basins" oriented normal to the main orogenic belt, "strike-slip basins" oblique to the orogenic strike [*Ori and Friend*, 1984; *Ricci-Lucchi*, 1986, 1987], or were developed as "detached basins" [*Steidtmann and Schmitt*, 1988].

[3] The fluviolacustrine sediments of the Kashmir valley, collectively known as the Karewa Group, consist of a sequence of ~1300-m-thick unconsolidated clay, sand, and conglomerate with lignite of the Pliocene to Pleistocene age that was deposited on Precambrian to fossiliferous Mesozoic basement rocks and is overlain by recent river alluvium [*Bhatt*, 1975, 1976; *Wadia*, 1976; *Singh*, 1982; *Burbank and Johnson*, 1982]. The cross-sectional exposures of this sequence are only observed along river sections and plateau margins of the Kashmir valley. The Karewa Group is best studied in sections located along the Rembiara and Romushi

[1]Indian Institute of Geomagnetism, New Panvel, Navi Mumbai, India.
[2]Institut für Geowissenschaften, Universität Tübingen, Tübingen, Germany.
[3]Physical Research Laboratory, Navrangpura, Ahmedabad, India.
[4]University of Jammu, Jammu Tawi, India.

0148-0227/10/2009JB006858

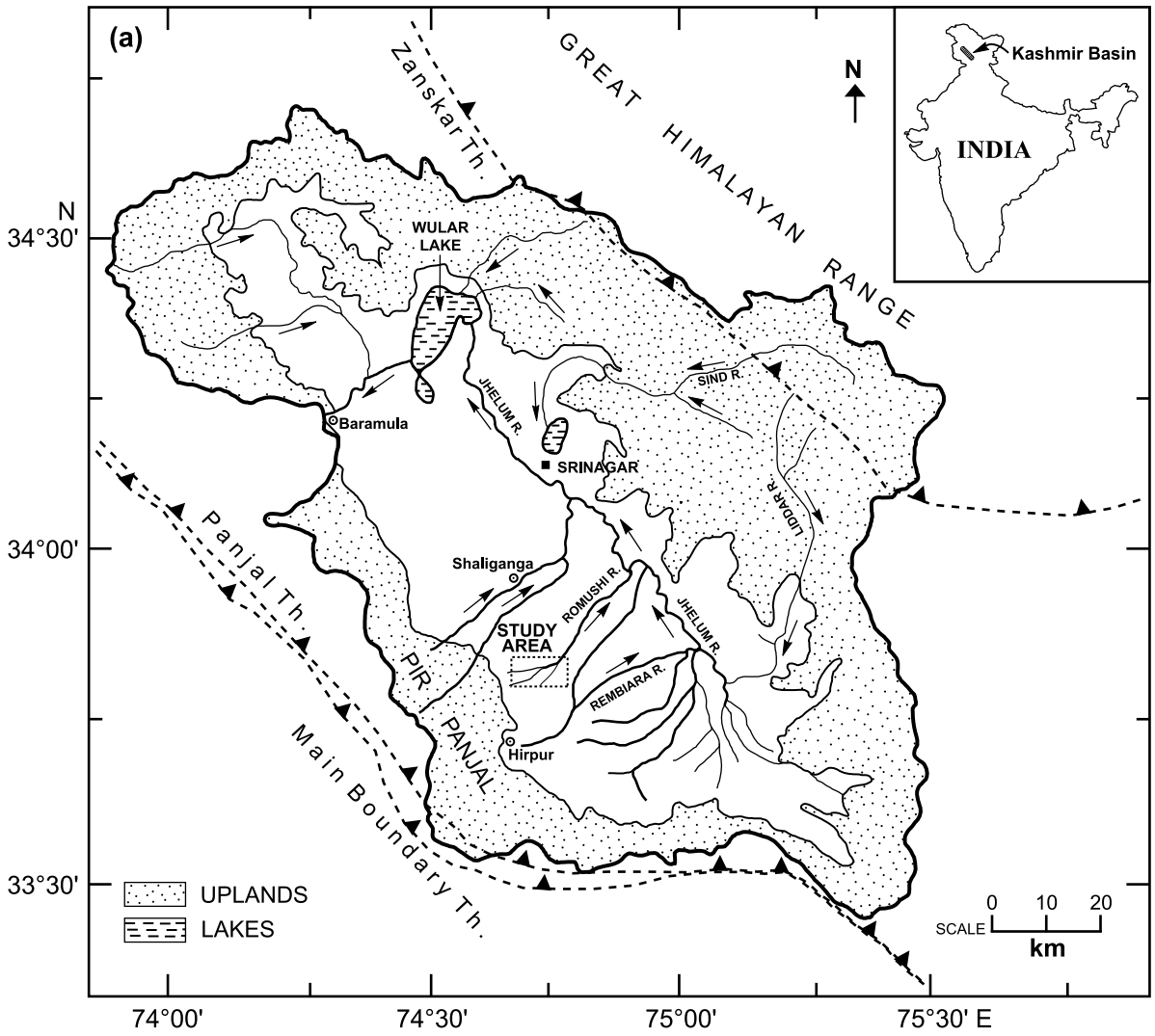
(a)
Zanskar Th.
GREAT HIMALAYAN RANGE
N
Kashmir Basin
INDIA
WULAR LAKE
JHELUM R.
SIND R.
Baramula
SRINAGAR
LIDDAR R.
Shaliganga
ROMUSHI R.
JHELUM R.
STUDY AREA
REMBIARA R.
Hirpur
Panjal Th.
PIR PANJAL
Main Boundary Th.
UPLANDS
LAKES
SCALE 0 10 20 km
N
34°30'
34°00'
33°30'
74°00'
74°30'
75°00'
75°30' E

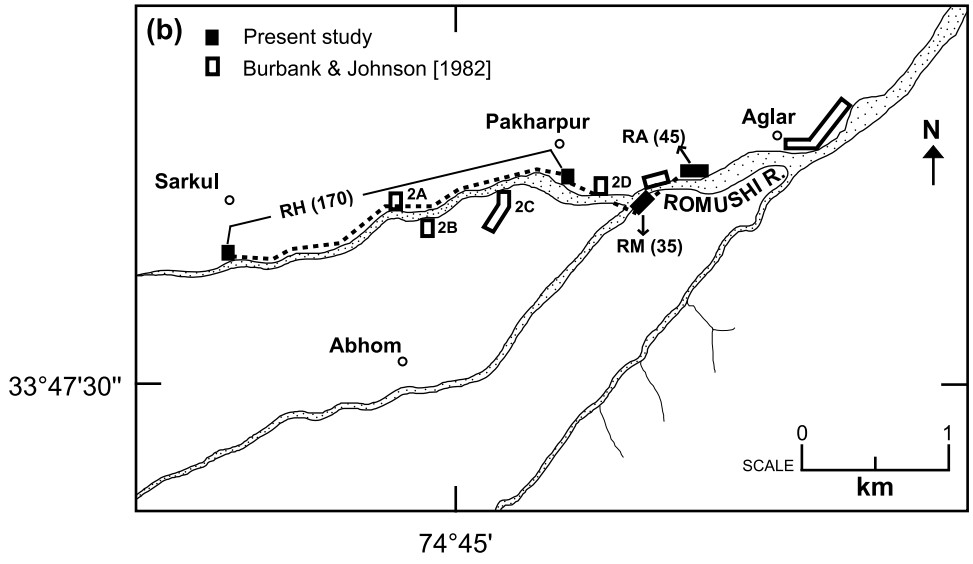
(b)
Present study
Burbank & Johnson [1982]
Pakharpur
RA (45)
Aglar
N
Sarkul
RH (170)
2A
2B
2C
2D
ROMUSHI R.
RM (35)
Abhom
SCALE 0 1 km
33°47'30"
74°45'

Figure 1

rivers, which constitute two of a few main tributaries of the northwesterly flowing Jhelum river that forms the main drainage system of the Kashmir valley (Figure 1a). The lower and upper halves of the ~1300-m-thick Karewa Group are exposed along the Rembiara and Romushi river sections, respectively. A marker volcanic ash horizon of 2.4 ± 0.3 Ma (Zircon fission track age; *Burbank* [1985]) or 2.3 ± 0.3 Ma [*Kusumgar et al.*, 1985] at the top of the Rembiara section was used to correlate these two sequences to get the whole stratigraphic succession of the Karewa Group. This marker volcanic ash horizon occurs in a triplet set in which each ash layer is 2 to 4 cm thick and the whole sequence occurs within a sedimentary thickness of 6 m [*Burbank and Johnson*, 1982]. The probable source of this volcanic ash is thought to be the Dasht-e-Nawar volcanic complex in east-central Afghanistan [*Johnson et al.*, 1982].

[4] The Kashmir valley sediments provide an important continental paleoclimate archive for past climatic reconstruction during the past ~4.0 Myr [*Agrawal*, 1985, 1988; *Agrawal et al.*, 1985, 1989]. The record of climate variability is preserved in both faunal and floral assemblages and has been successfully utilized by the earlier workers [*De Terra and Paterson*, 1939; *Bhatia*, 1968; *Badam*, 1972; *Roy*, 1975; *Tewari and Kachroo*, 1977; *Bhatia et al.*, 1985; *Bhatt*, 1989]. In addition to this, the sequence preserves valuable information about the evolution of a synorogenic sedimentary basin within an active orogenic belt [*Bhatt*, 1989; *Agarwal and Agrawal*, 2005].

[5] The major objective for the present research is the determination of a reliable magnetostratigraphic age frame for the Karewa Group. Earlier magnetostratigraphic work by *Burbank and Johnson* [1982] identified five normal and five reversed polarities in the magnetic polarity sequence from the Rembiara river (Hirpur section) and Romushi river sections (Figure 1a). Their results indicate that the Hirpur section of the Rembiara river spans from the late Gilbert to early Matuyama chrons (~3.80 to 1.97 Ma), whereas the Romushi river section covers most of the Matuyama and Brunhes chrons (from 2.48 to 0.3 Ma). *Burbank and Johnson* [1982] also suggested a gradually decreasing sediment accumulation rate (SAR) from the bottom to the top of the Karewa Group. These SARs were estimated at 50 cm kyr^{-1} for the lower ~850 m of the sedimentary sequence (Gilbert and Gauss chrons), 32 cm kyr^{-1} for the ~250-m-thick middle part (early and middle Matuyama chron), and 16 cm kyr^{-1} for the topmost ~300 m (upper Matuyama and Brunhes chrons). However, these conclusions need further evaluation because the ~200- to 300-m-thick conglomerate horizon in the lower Karewa Group represents a rapid depositional sequence unlike the other fluviolacustrine members of this group [*Burbank and Johnson*, 1983].

[6] Because of acute lack of resources to carry out any systematic scientific work in the region, no significant research work could be objectively taken up in the Kashmir valley from about 1990 until recently. The motivation for the present work has been to essentially reevaluate the SARs for the Kashmir basin from a sequence of the Romushi river section using magnetic polarity chrons for visual comparison and correlation among subsections of this valley. The temporal changes in SARs are used to understand the role and the interplay between tectonics and the climatic variability. In addition, we also present anisotropy of magnetic susceptibility (AMS) data from this sedimentary sequence to help in understanding the changes in paleocurrent directions in Kashmir valley that occurred during the Pliocene-Pleistocene time. AMS studies have been published for fluvial sediments [*Ellwood*, personal communication, in *Tarling and Hrouda*, 1993; *Gautam and Rösler*, 1999; *Gautam et al.*, 2000; *Sangode et al.*, 2001; *Hrouda*, 2007] and glaciolacustrine sediments [*Kodama et al.*, 1985; *Rosenbaum et al.*, 2000; *Soto et al.*, 2009]. However, examples of fluviolacustrine sequences are rare in the literature [*Garćes et al.*, 1997].

2. Stratigraphy and Sampling

[7] The sediments of the Karewa Group have been subdivided into the progressively younger Hirpur, Nagum, and Dilpur formations, respectively [*Bhatt*, 1989]. The Hirpur Formation broadly consists of gray to bluish-gray clay, light-gray sandy clay, fine to coarse-grained green to purple sand, conglomerate, lignite, and lignitic clay. The Nagum Formation is made up of fine to coarse-grained greenish to purplish sand, gray and ochre sandy clay, ochre and cream-colored marl and gravel. The upper Dilpur Formation mostly consists of brown silt.

[8] Samples for paleomagnetic studies were collected in 8 cm^3 cylindrical plastic containers using a portable soft sediment corer and were oriented using a magnetic compass. In total, 250 samples were collected from 440-m-thick sediment succession along the Romushi river. For stratigraphic continuity, a volcanic ash bed at 110-m height was used as a marker horizon that allowed for reconstructing a composite sedimentary sequence. Along the Romushi river, the lower stratigraphic level was exposed close to Pir Panjal near the Sarkul village (33°48′05″N, 74°43′00″E), and as we moved eastward the higher stratigraphic levels were exposed (Figure 1b). The sampled section covers the magnetic chrons between 4.40 and 0.77 Ma, when compared to *Burbank and Johnson* [1982, 1983] and *Agrawal et al.* [1989]. Samples of texturally fine-grained sediment such as silt and clay were collected, whereas pedogenically altered and anthropogenically disturbed horizons were avoided.

[9] Our sampled sections are named as RH, RM, and RA (Figure 1b) from older to younger in stratigraphic succession. The lithology of these sections is summarized in Figure 2. We collected 170 samples from RH section dominated by laminated bluish to gray clay and sandy/silty clay with occasionally intercalated thin carbonaceous clay. A thick unconsolidated bed (~30-m thick) followed by a volcanic ash horizon occur in the upper half of the succession between ~110 and 180 m. From RM section, 35 samples were collected. This section consists of alternating relatively

Figure 1. (a) Present study area of Kashmir valley showing the Jhelum river and its main tributaries Rembiara and Romushi, upland regions, and the present lakes. (b) Simplified sketch map of the Romushi river cross section. Locations of our sampling sections RH, RM, and RA are shown by the dotted line and black boxes. Number of samples at RH, RM, and RA are given in brackets. White boxes are sampling localities of *Burbank and Johnson* [1982].

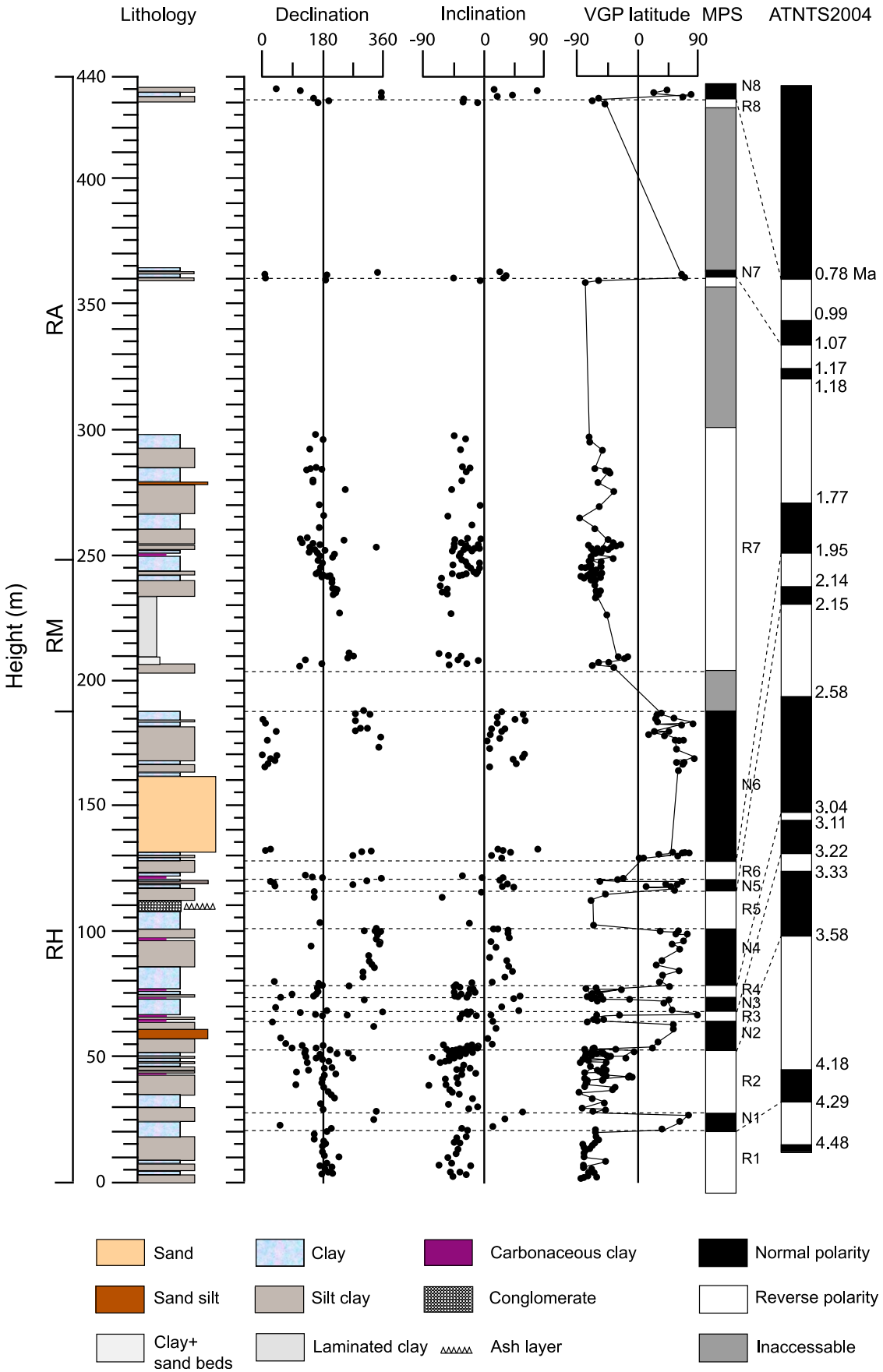
Lithology
Declination
Inclination
VGP latitude
MPS
ATNTS2004
0
180
360
-90
0
90
-90
0
90
Height (m)
RA
RM
RH
440
400
350
300
250
200
150
100
50
0
N8
R8
N7
R7
N6
R6
N5
R5
N4
R4
N3
R3
N2
R2
N1
R1
0.78 Ma
0.99
1.07
1.17
1.18
1.77
1.95
2.14
2.15
2.58
3.04
3.11
3.22
3.33
3.58
4.18
4.29
4.48
Sand
Clay
Carbonaceous clay
Normal polarity
Sand silt
Silt clay
Conglomerate
Reverse polarity
Clay+ sand beds
Laminated clay
Ash layer
Inaccessable

Figure 2

thick beds of bluish to gray clay and silty clay. Sandy silt and carbonaceous clay are generally absent in RM, but thin sandy beds are occasionally present. From RA section, 45 samples were collected. The section consists of bluish to gray clay and silty, clayey beds with carbonaceous clay with occasional sandy silt. A major part of this section could not be sampled due to inaccessibility.

3. Experimental Procedure

[10] Laboratory analyses for paleomagnetic and rock magnetic investigations were carried out at the Indian Institute of Geomagnetism, Navi Mumbai, India, and at Tübingen University, Germany. Paleomagnetic measurements were made using a 2G Enterprises RF-SQUID and AGICO JR6 and Molspin spinner magnetometers. Alternating field (AF) demagnetization was carried out in 17 steps up to a peak field of 140 mT using a Molspin AF demagnetizer and a 2G600 automatic degaussing unit attached to the SQUID system. To examine the application of the most suitable procedure, a thermal demagnetization was carried out on a few samples in a μ-metal shielded MMTD80 furnace (Magnetic Measurements Ltd.). However, in our experiments, AF demagnetization was found to be more effective than thermal demagnetization, because the behavior of the samples during stepwise thermal demagnetization is found to be diverse and often unstable. Hence, AF demagnetization provides well-determined linear segments in the Zijderveld diagrams and could well discriminate the characteristic remanent magnetization (ChRM) of magnetite. Orthogonal vector plots and equal area projections were used to examine the AF demagnetization behavior of the specimens. The components of the NRM vector were isolated using principal component analysis [*Kirschvink*, 1980].

[11] Magnetic mineralogy was investigated on representative specimens using the following procedure:

[12] 1. Isothermal remanent magnetization (IRM) acquisition curves in steps from 10 to 2500 mT;

[13] 2. Backfield application to the saturation IRM (SIRM) and evaluation of the remanent coercive force (H_{cr});

[14] 3. Stepwise thermal demagnetization of SIRM carried out in a MMTD80 furnace between 100°C and 700°C in discrete steps of 25°C and 50°C, and a MMPM9 pulse magnetizer (Magnetic Measurements Ltd) with a maximum field of 2.5 T was used for inducing an IRM;

[15] 4. Temperature dependence (−200°C to 700°C) of magnetic susceptibility measured in argon atmosphere by a CS3 unit coupled to an AGICO KLY-4S Kappabridge;

[16] 5. SIRM thermal alteration tests similar to those undertaken by *Van Velzen and Zijderveld* [1992], involving the sample be initially given a saturation IRM (SIRMleft) and remagnetized in the same field after each thermal step 2T IRM (2T SIRM); and

[17] 6. Hysteresis data using a Molspin Nuvo vibrating sample magnetometer in fields cycling between ±1 T.

[18] Measurement of low-field (300 Am^{-1} at 920 Hz) AMS was carried out using a Kappabridge KLY-4S for each specimen with measurement in 64 directions on three mutually orthogonal planes using an automatic rotator sample holder. The azimuths and magnitudes of principal susceptibility axes (K_{max}, K_{int}, and K_{min}) were calculated using SUFAR software supplied by AGICO, together with other magnetic anisotropy parameters such as anisotropy ratios, expressed as corrected degree of anisotropy (P′), shape (T), magnetic lineation (L), and magnetic foliation (F). The AMS data were analyzed by Jelinek (P′-T) and Flinn (F-L) bivariate plots. The equations used in calculating these parameters can be found in *Tarling and Hrouda* [1993].

4. Results

4.1. Magnetic Mineral Carriers

[19] Tables 1 and 2 summarize the concentration-, grain size-, and composition-dependent parameters and parameter ratios for a representative subset that covers the whole Romushi section. Figure 3a plots χ versus SIRM values (bilogarithmic plot) for the full set of samples studied. Figures 3b–3j shows typical curves for IRM acquisition and backfield, SIRM behavior during thermal demagnetization, SIRM thermal alteration tests, behavior of low- and high-temperature χ-T curves, and a Day plot of M_{rs}/M_s versus H_{cr}/H_c.

[20] For most samples, <95% of saturation is achieved at ~200 to 300 mT, indicating a predominantly low coercivity mineral contribution. This is supported by H_{cr} values ranging from 40 to 85 mT (Figure 3b). The IRM unblocking temperatures between ~100°C and 300°C indicate the presence of Ti-rich titanomagnetites (Figure 3c). Some magnetite and possibly a small contribution of hematite are evident by maximum IRM unblocking temperatures at ~580°C and above 680°C, respectively.

[21] During SIRM tests, all samples show a similar behavior with a large IRM drop in SIRMleft at 300°C reflecting Ti-rich titanomagnetite, and the presence of magnetite and hematite are shown by small drops at ~580°C and ~700°C, respectively (Figures 3d–3f). High temperature χ-T curves (Figures 3g–3i) display an increase in susceptibility with temperature before dropping significantly at ca. ~300°C, then rises followed by a sharp drop at ~580°C. The two drops in susceptibility at ~300°C and ~580°C indicate the occurrence of titanomagnetite and magnetite, respectively. The increase of χ between room temperature and the Curie temperature is very typical for Ti-rich titanomagnetite [*Appel and Soffel*, 1985]. The irreversibility of cooling curve may be caused by destruction of Ti-rich titanomagnetite (exsolved into magnetite-near and ilmenite-near phases). Low temperature χ data (Figures 3g–3i) show the presence of the peak just above the Verwey transition, typically caused by the isotropic point of magnetocrystalline anisotropy, suggesting multidomain (MD) magnetite. Hysteresis parameters plotted on the Day plot (Figure 3j) indicate a predominant MD or in some cases large pseudo-single domain (PSD) grains. However, this interpretation has to be consid-

Figure 2. Composite litholog of RH, RM, and RA parts of the Romushi river section plotted together with declination, inclination, and virtual geomagnetic pole (VGP) latitudes. The magnetic polarity sequence (MPS) from the composite Romushi river section is correlated with the reference Astronomically Tuned Neogene Time Scale (ATNTS2004) [*Lourens et al.*, 2004].

Table 1. Summary of Mineral Magnetic Measurements of Romushi River[a]

		Concentration			Grain size		Composition		
Height m	NRM 10^{-7} Am^2 kg^{-1}	χ 10^{-8} m^3 kg^{-1}	ARM 10^{-5} Am^2 kg^{-1}	SIRM 10^{-5} Am^2 kg^{-1}	ARM/SIRM k	SIRM/χ k A/m	Soft IRM 10^{-5} Am^2 kg^{-1}	Hard IRM 10^{-5} Am^2 kg^{-1}	S ratio
230–435 m									
362	22.9	37.9	0.05	437.1	0.11	11.5	274.7	31.5	0.93
360	60.1	51.9	0.14	530.8	0.26	10.2	391.1	161.0	0.70
283	10.3	15.5	0.04	40.1	1.00	2.6	32.6	22.8	0.43
255	36.6	74.3	0.09	370.4	0.24	5.0	59.1	12.6	0.97
248	34.2	33.7	0.13	298.5	0.44	8.9	125.6	24.5	0.92
243	22.1	28.6	0.18	161.2	1.12	5.6	65.9	25.2	0.84
241	314.5	79.9	0.22	819.7	0.27	10.3	246.3	0.4	0.99
130–230 m									
226	91.2	46.1	0.15	346.7	0.43	7.5	98.8	24.5	0.93
208	12.2	39.8	0.20	357.8	0.56	9.0	113.8	23.9	0.93
205	7.8	22.9	0.06	108.9	0.55	4.8	41.3	18.1	0.83
167	27.8	59.5	5.97	545.4	10.95	9.2	401.0	62.5	0.89
29–130 m									
130	13.7	41.5	0.76	224.7	3.38	5.4	82.5	13.2	0.94
75	27.2	15.0	0.48	64.6	7.43	4.3	15.7	1.3	0.98
68	45.2	43.1	0.71	389.6	1.82	9.0	281.4	4.3	0.99
48	1.9	10.5	1.03	37.3	27.61	3.6	4.8	0.4	0.99
36	86.2	54.6	1.12	840.1	1.33	15.4	708.3	183.8	0.78
0–29 m									
23	44.3	41.1	0.72	641.3	1.12	15.6	428.7	212.8	0.80
14	95.9	65.4	0.62	768.5	0.81	11.8	467.7	132.9	0.83
0.5	89.9	35.6	1.37	380.2	3.60	10.7	306.2	71.7	0.81

[a]NRM, natural remanent magnetization; χ, magnetic susceptibility; ARM, anhysteretic remanent magnetization; SIRM, saturation isothermal remanent magnetization; Soft IRM, SIRM–IRM_{-30mT}; HIRM, SIRM–IRM_{-300mT}, and S-ratio, IRM_{-300mT}/SIRM.

ered with caution as, in a strict sense, conclusions from the Day plot are only valid for single-phase samples. The presence of titanomgnetite is likely, considering that the Pir Panjal Trap sequence exists near the sampling sites, serving as a source area for the sediments in the Romushi river section.

[22] Alternative explanations for the prominent IRM decay between ~100°C and 300°C are less likely. These include maghemite destruction, which generally occurs at higher temperatures (above 300°C to 400°C), or greigite alteration, but a significant decay <200°C is unusual. SIRM/χ ratios are low through the entire section (2.6 to 15.6 kAm^{-1}) (Table 1) and which are contradictory to the occurrence of greigite [*Reynolds et al.*, 1999]. In addition, this loss might be due to the presence of fine-grained hematite, being single domain at room temperature and reaching the superparamagnetic state at low elevated temperatures. Nevertheless, we expect a harder magnetic behavior during IRM acquisition and higher H_{cr} values.

[23] A good linear correlation between χ and SIRM (Figure 3a) and the comparison of low-field susceptibility

Table 2. Summary of Hysteresis Measurements of Romushi River Section[a]

Height m	χlow 10^{-8} m^3 kg^{-1}	χhigh 10^{-8} m^3 kg^{-1}	χferri 10^{-8} m^3 kg^{-1}	χferri%	χhigh%	M_s 10^{-3} Am^2 kg^{-1}	M_{rs} 10^{-3} Am^2 kg^{-1}	H_c mT	H_{cr} mT
230–435 m									
362	287.1	10.6	276.5	96.3	3.7	51.6	12.8	26.7	74.9
360	44.5	10.9	33.6	75.4	24.6	1.5	1.1	26.7	82.9
255	277.5	2.6	274.9	99.0	1.0	140.6	6.6	6.1	38.7
248	90.9	15.7	75.1	82.7	17.3	32.9	3.3	15.6	61.6
243	129.6	13.9	115.7	89.3	10.7	39.7	2.9	7.8	33.3
241	333.9	1.6	332.2	99.5	0.5	161.5	13.8	11.1	49.3
130–230 m									
226	112.3	12.7	99.6	88.7	11.3	43.2	5.4	13.3	49.3
208	108.6	16.5	92.1	84.8	15.2	36.2	4.9	14.4	46.1
205	81.8	13.2	68.6	83.8	16.2	15.3	1.8	7.8	23.7
167	183.5	10.3	173.2	94.4	5.6	83.8	6.6	12.2	85.6
29–130 m									
130	161.0	11.2	149.7	93.0	7.0	53.8	3.7	7.8	37.1
68	158.2	11.9	146.3	92.5	7.5	42.4	5.4	12.8	64.3
36	164.9	12.2	152.7	92.6	7.4	38.4	6.9	19.4	63.7
0–29 m									
23	1404.5	21.2	1383.2	98.5	1.5	206.6	37.6	11.1	78.1
14	409.1	2.6	406.5	99.4	0.6	135.3	17.1	18.0	74.9
0.5	142.4	11.7	130.7	91.8	8.2	39.4	6.5	16.7	165.6

[a]χlow, low field susceptibility; χhigh, high field susceptibility; χferri, difference between χlow and χhigh; χferri%, percentage of ferromagnetic contribution; χhigh%, percentage held in paramagnetic and high coercive antiferromagnetic phases; M_s, saturation magnetization; M_{rs}, saturation remanent magnetization; H_c, coercivity; and H_{cr}, coercivity of remanence.

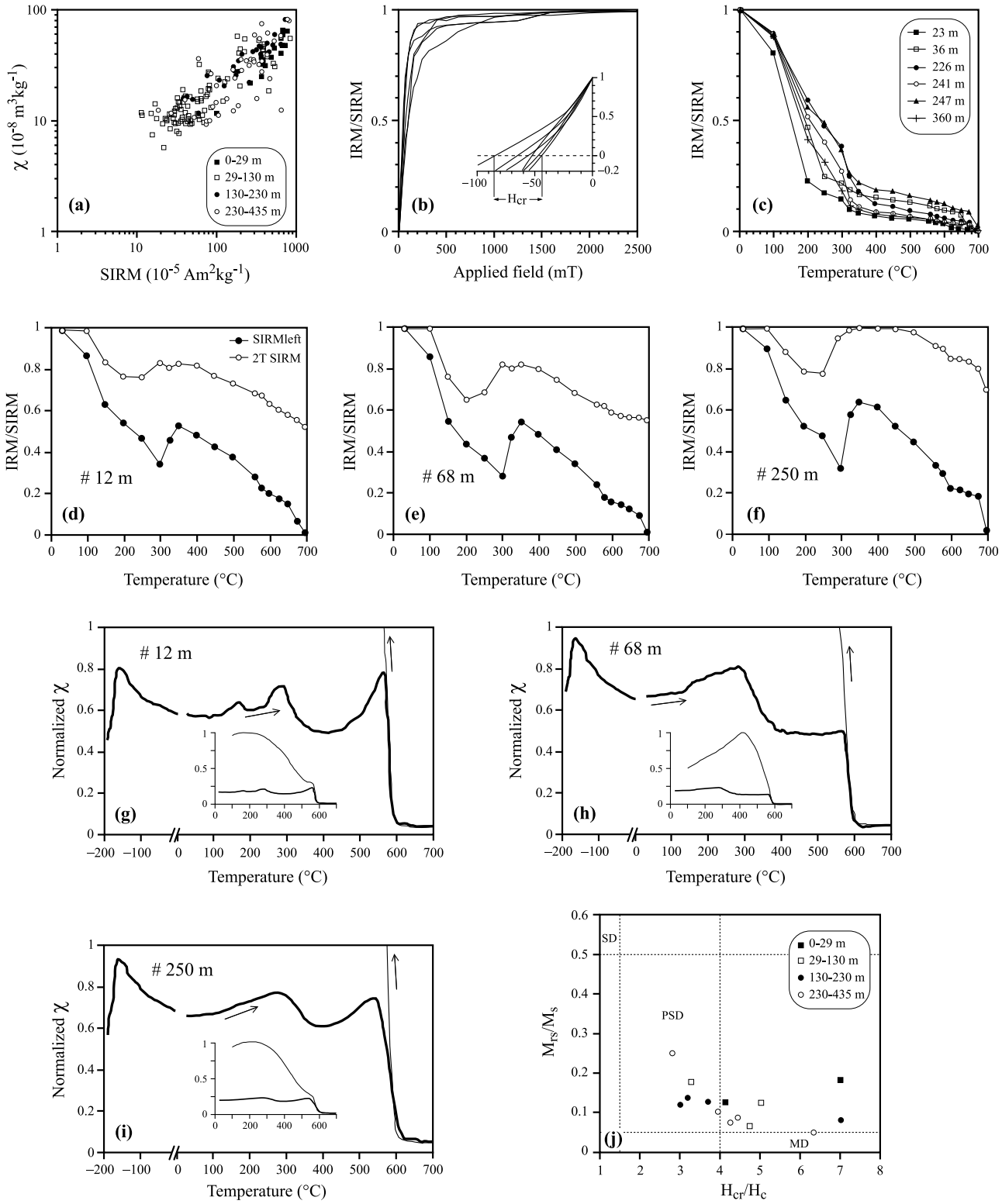

Figure 3. Typical examples of (a) bilogarithmic plot of the magnetic susceptibility versus the saturation remanent magnetization for the full set of samples, (b) acquisition of isothermal remanent magnetization and backfield demagnetization, (c) progressive thermal demagnetization of the saturation IRM, (d–f) thermal demagnetization of 2 T SIRM and SIRMleft after each 2 T SIRM induction, (g–i) magnetic susceptibility versus temperature (−200°C to 700°C) curves, and (j) Day plot of M_{rs}/M_s versus H_{cr}/H_c. Note different symbols represent four sampling levels of 0–29 m, 29–130 m, 130–230 m and 230–435 m classified according to their AMS characteristics.

determined by Kappabridge and high-field susceptibility determined by the slope of hysteresis curves at higher fields prove a dominant contribution of ferrimagnetic minerals to the magnetic susceptibility, also demonstrating that AMS is controlled by ferromagnetic minerals (Table 2). S ratios are mostly >0.92, confirming that Ti-rich titanomagnetite and magnetite are the principal magnetic carriers. The samples between 0 and 29 m contain an appreciable amount of hematite as seen from S ratio (mean 0.82) and relatively high Hard IRM values. Results shown in Figure 3 and the data in Tables 1 and 2 are consistent with magnetic mineral assemblages, in which MD and PSD Ti-rich titanomagnetite, magnetite, and hematite are present in varying relative proportions.

4.2. Remanence Directions and Magnetostratigraphy

[24] Typical examples of endpoint vector diagrams for AF demagnetization of 250 samples are shown in Figure 4. From 205 samples, the vector projections indicate a well-defined component of ChRM by a linear decay toward the origin. Soft magnetization components were also observed in several samples. These components were removed by AF fields of 5–15 mT (Figures 4a, 4b, 4f, 4g, and 4h). These soft components are mostly found in the N1 polarity of the Gilbert, N2 and N3 of the Gauss, and in N5 and R7 polarity of the Matuyama chrons (Figure 2).

[25] The direction of ChRMs was determined from orthogonal plots in at least five successive measurement steps between 20 and 80 mT using the principal component analysis (PMAGIC software; [*Rehacek*, 1994]) (Figure 4). The maximum angular deviations are <5°. From all the studied samples, nearly 205 samples yielded significant ChRM directions, which have a mean normal polarity of $D_m = 349.6°$, $I_m = 38.6°$, $k = 3.8$, $\alpha_{95} = 10.6$ ($N = 63$), and a mean reversed polarity of $D_m = 172.5°$, $I_m = -39.5°$, $k = 6.6$, $\alpha_{95} = 5.0$, ($N = 142$) (Figure 5). For evaluating the consistency in the determination of normal and reversed polarities of Romushi section, reversal test was performed following *McFadden and McElhinny* [1990]. The angle (γ_o) between the mean directions of normal and reversed polarities is determined as 2.9°, which is smaller than the critical angle (γ_c) of 10.4°. Consequently, the reversal test is positive and belonging to the quality classification C. The remaining 45 samples from profiles RH ($N = 28$), RM (9) and RA (8) (Figure 1b) show somewhat random directions during demagnetization, and hence they are not considered further in the present study.

[26] Declination, inclination, and calculated virtual geomagnetic pole (VGP) latitude are shown in Figure 2 for evaluating the magnetostratigraphy of the Romushi river section. In all, magnetozones of eight normal and eight reversed polarities have been identified by us on the basis of a comparison of the latest Astronomically Tuned Neogene Time Scale (ATNTS2004) published by *Lourens et al.* [2004], which suggests that the Romushi river section falls between 4.40 and 0.77 Ma (Figure 2). Major chrons identified by us and by the work of *Burbank and Johnson* [1982] in the Romushi river sections are the upper Gilbert (close to 3.58 Ma), Gauss (3.58–2.58 Ma), Matuyama (2.58–0.77 Ma), and lower Brunhes (<0.77 Ma). However, the following additional subchrons were identified (Figure 6) within the Romushi river composite section in our study: (1) the Cochiti and its preceding and succeeding reversed subchrons, (2) the Mammoth and its preceding and succeeding normal subchrons and Kaena subchrons, and (3) the Jaramillo subchron in the Matuyama chron.

4.3. Anisotropy of Magnetic Susceptibility

[27] In the stratigraphic sequence of the Karewa Group [*Burbank and Johnson*, 1982, 1983; *Agrawal et al.*, 1989; *Bhatt*, 1989], there are some important marker horizons or sedimentary sequences that may indicate marked changes in the environment during sediment deposition in the Kashmir basin during Pliocene-Pleistocene (Figure 7). The most important of these is the 200- to 300-m-thick conglomerate horizon at the bottom of the Rembiara river section [*Burbank and Johnson*, 1982]. Although, the Karewa Group is considered to be fluviolacustrine in origin [*Bhatt*, 1975, 1976; *Wadia*, 1976; *Burbank and Johnson*, 1982; *Singh*, 1982], this conglomeratic horizon is thought to have been deposited during tectonic uplift of the Pir Pangal range and the consequent rejuvenation of fluvial transport [*Bhatt and Chatterji*, 1976; *Burbank and Johnson*, 1982; *Bhatt*, 1989]. The next phase of tectonomagmatic activity that might have important bearing on the style of sedimentation of the Karewa Group was perhaps the triplet volcanic ash horizon identified by *Burbank and Johnson* [1982].

[28] For the purpose of characterization and classification on the basis of grain size and thickness of sedimentary beds, we divided the composite section into three parts (Figure 7). The lowest part extends from the base of the section to 130-m height that includes the volcanic ash horizon and another 20-m-thick sequence of silty clay above the ash horizon. This oldest portion of the sequence includes mostly moderate thick layers of clay and silty clay sediments. The second part from ~130 to 230 m is mostly characterized by thick beds of sand and clay separated by thin sedimentary layers. The third and highest part in the section from ~230 to 300 m contains relatively thin sediment beds of silty clay and clay. We also collected two short intervals much higher in the section, which were used in the polarity study but not in the AMS analysis because of a fewer number of samples.

[29] To interpret the AMS fabric of Karewa Group sediments, our data are compared mostly with existing theoretical and experimental studies concerning the depositional fabric of sediments during current flow or in still water [*King*, 1955; *Granar*, 1958; *Hamilton and Rees*, 1970; *Rees and Woodall*, 1975; cf. *Tarling and Hrouda*, 1993]. In the fluvial environment, minimum susceptibility axes (K_{min}) always orient perpendicularly to the flow direction on a near-horizontal depositional surface irrespective of weak to moderate (less than ~1 cm sec^{-1}) or strong (greater than or equal to ~1 cm sec^{-1}) current velocity. The K_{max} axes will be either parallel or perpendicular to the direction of flow when the current is either weak to moderate or strong, respectively [*King*, 1955; *Granar*, 1958; *Rees and Woodall*, 1975]. The resultant shape of AMS ellipsoid of sediments is therefore prolate in fluvial environment. Fluvial experiments on flat surface [*Rees and Woodall*, 1975] can be used to interpret our results in fluviolacustrine environment (Figure 1a) because the depositional surface in the center of the Kashmir basin supposedly had a very gentle slope [cf. *Burbank and Johnson*, 1982, 1983]. The resultant shape of the AMS ellipsoid of fine sediments in still water is usually an oblate

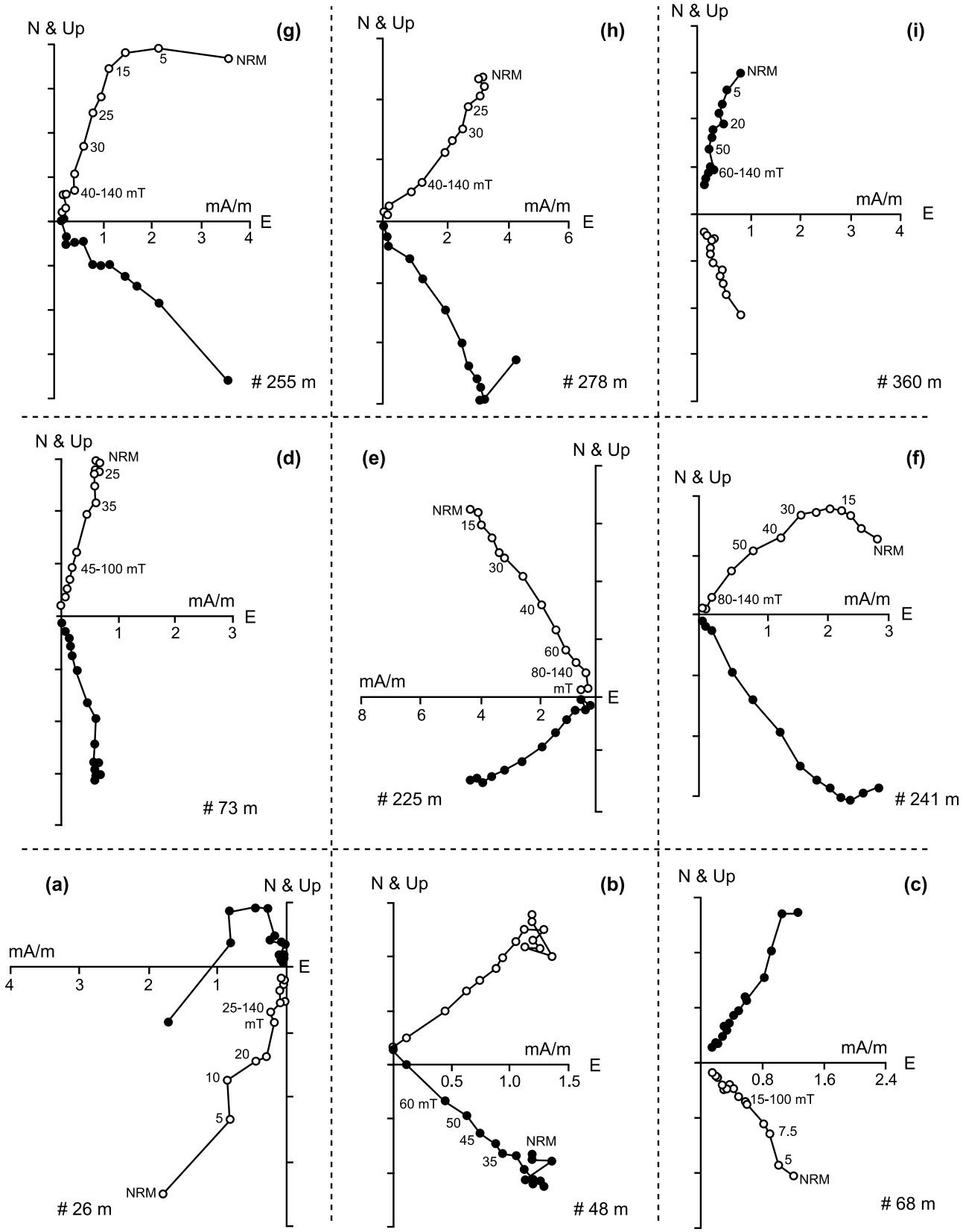

Figure 4. Orthogonal vector plots of AF demagnetization of representative samples at different levels. Solid (open) circles are horizontal (vertical) projections of remanent magnetization vectors at various steps of demagnetization. #,stratigraphic levels of the samples in the section.

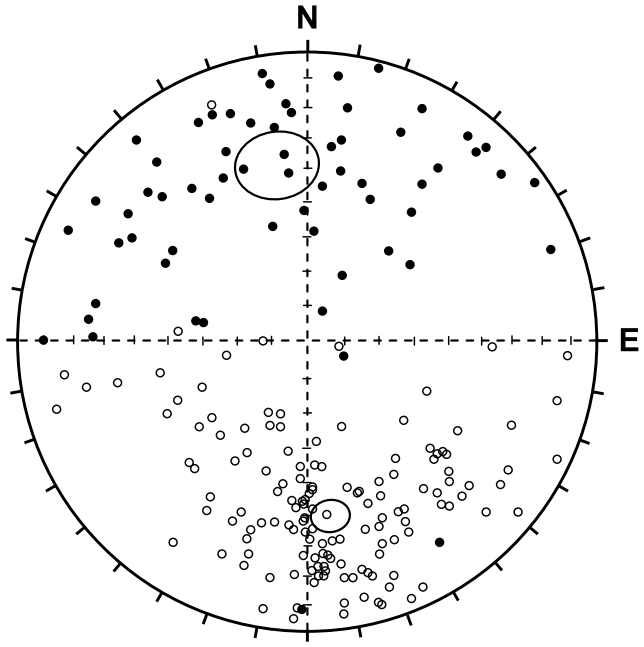

Figure 5. Equal area projection of site mean characteristic directions of the Karewa Group from Romushi River cross section. Solid (open) circles are projections on the lower (upper) hemisphere.

fabric. At the same time, superimposition of some anisotropy on this shape is possible if elongated grains roll on the shallowly sloping depositional surface and are preferentially aligned perpendicular to the slope [*Tarling and Hrouda*, 1993].

[30] The K_{max} and K_{min} axes are plotted within the stratigraphic framework of the composite Romushi river section in Figure 7. The K_{min} axes for the samples from the base of the section to 29 m height show two dominant orientations of K_{min} axes in the NE and NW directions with clustering of respective K_{max} axes (Figure 7a). The K_{min} axes of the sediment section above 29–130 m are mostly vertical to subhorizontal and show a NE–SW trending major orientation, although a large scatter is observed (Figure 7b). The respective K_{max} axes from this part of the section are mostly subhorizontal and show concentrations primarily in the SE and NW sectors. However, there is also a minor concentration of K_{max} axes in the SW sector along the trend of the K_{min} axes. In the P′ versus T plots (Figures 8a–8b), a minor concentration in the prolate quadrant with relatively low P′ values (<1.02) is noticed for the lowest sediment succession up to 29 m height. The succeeding sedimentary succession from 29 to 130 m height describes a cluster of AMS data in the oblate field whereas P′ varies up to ~1.08, and there is a diffused increasing trend of P′ with increasing T. In the F versus L plots, most of the data points from the sedimentary succession from ~29 to 130 m height are clustered in the oblate field (Figures 8a–8b).

[31] The middle part between 130 and 230 m, which is dominated mostly by relatively thick sedimentary layers (Figure 7c), shows a NE–SW trend of vertical to inclined K_{min} axes with subhorizontal K_{max} axes concentrating mostly in the ESE and WNW quadrants, similar to that in the 29 to 130 m section. In P′ versus T plots, most of the data are in the oblate field. These data show two prominent concentrations, one at low P′ value (<1.04), and the other at relative high P′ value between ~1.06 and 1.10 (Figure 8c). The distribution of data in the F versus L plots show two different linear trends with moderate and relatively steep slopes, respectively (Figure 8c).

[32] However, the younger sequence in respect of the top section between ~230 and 300 m, reveals a sudden change in orientation of vertical to subvertical K_{min} axes toward the NW–SE trend, although we suggest that the NW component predominated (Figure 7d). The corresponding K_{max} axes are subhorizontal and show concentration in the SE sector. In the P′ versus T plots, the top section data are plotted in the oblate field with two distinct groupings (Figure 8d); the data with $P' < 1.04$ show point concentration and those having P′ between ~1.06 and 1.10 show a linear increasing trend with moderate slope. In the F versus L plot, however, all data points show a distinct increasing linear trend with a moderate slope (Figure 8d).

5. Discussion

5.1. Dating of the Karewa Group

[33] The Romushi river section of the Karewa Group has been used to reevaluate the reported changes in polarity during Gilbert to Brunhes chrons. In addition to the established five normal and five reversed polarities in the Pliocene-Pleistocene in the Kashmir valley [*Burbank and Johnson*, 1982], we have identified seven additional subchrons, namely (1) the Cochiti and its preceding and succeeding reversed subchrons dated between 4.40 and 3.58 Ma, (2) the Mammoth and its preceding and succeeding normal subchrons and Kaena subchrons between 3.58 and 2.58 Ma, and (3) the Jaramillo subchron dated at 1.07 to 0.99 Ma in the Matuyama chron. In the earlier study, the Hirpur and Romushi river sections were combined to reconstruct the magnetostratigraphy of the Kashmir valley [e.g. *Burbank and Johnson*, 1982; *Kusumgar et al.*, 1985]. However, this study demonstrates that the Romushi section has a complete record of sediment aggradation from 4.40 to 0.77 Ma (Figure 2). The new set of magnetostratigraphic data generated in the present study shows the presence of eight normal (N1 to N8) and eight reversed (R1 to R8) polarity intervals, known for the first time from Kashmir intermontane basin and thus providing a most comprehensive chronology for the Pliocene-Pleistocene epoch (Figure 2).

5.2. Variation in Paleocurrent Direction

[34] *Burbank and Johnson* [1983] argued that sedimentation in the Kashmir basin commenced at ~4.40 Ma, resulting in the buildup of a ~1300-m-thick sequence of sediments deposited in a low-energy fluviolacustrine environment. This was punctuated by conglomerate horizons eroded in pulses from the faulted basin margins at ~3.5 to 3.0, 2.7, 2.1, and 1.7 Ma. On the basis of paleocurrent data, *Burbank and Johnson* [1983] suggested that the lowermost fluvial gravels (~4.0 Ma) were deposited by rivers that emanated from the NE and E (Himalayan flank) and owe their genesis to the pulsed tectonic activity along the northeastern margin of the Kashmir basin. However, in the overlying succession, paleocurrent data collected within the deltaic and fluvial sequences at Hirpur, Romushi, and Shaliganga areas

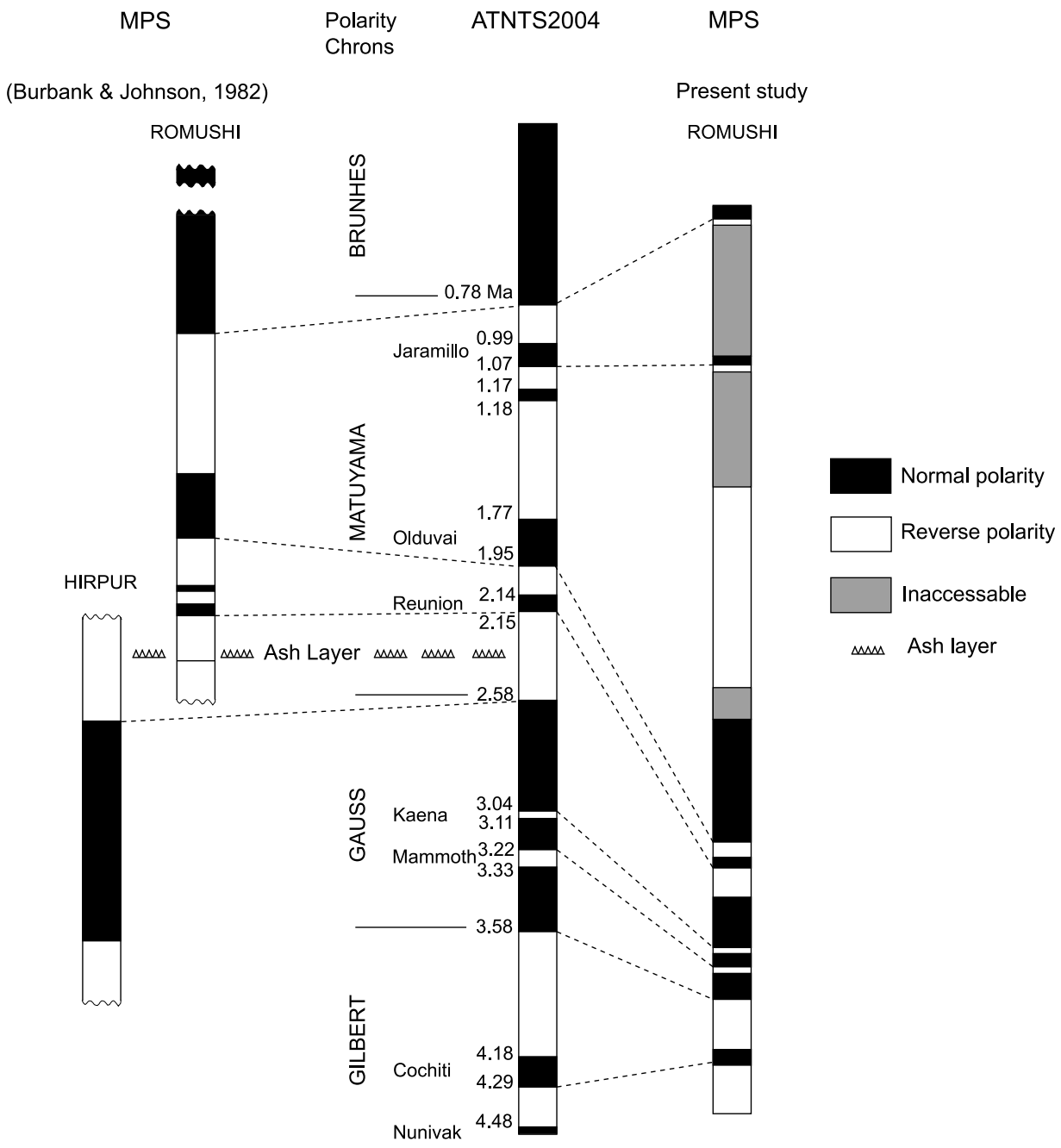

Figure 6. Chronostratigraphic correlation between MPS of Romushi and Hirpur sections of [*Burbank and Johnson* 1982], together with the present MPS results from Romushi section and their correlation with the latest ATNTS [*Lourens et al.*, 2004].

(Figure 1a) indicated N and NE flow (away from Pir Panjal) [*Burbank and Johnson*, 1983].

[35] The AMS data obtained from Romushi section between the base and 29 m height (dominated by clay and silty clay) correspond to the middle Gilbert chron (~4.40 and 4.18 Ma) (Figure 7). The prolate shaped AMS ellipsoids (Figures 8a, 8b) suggest the deposition under a fluvial environment in the Kashmir valley [*Tarling and Hrouda*, 1993]. The overlying sequence between ~29 and 130 m height (upper Gilbert, Gauss, and lower Matuyama chrons), however, shows oblate AMS ellipsoids (Figures 8a–8d), which are indicative of the prevalence of a lacustrine environment.

[36] Although the majority of succession studied shows an oblate AMS ellipsoid (Figure 8) that is typical for lacustrine deposits, the distribution of their K_{min} axes provides insight into the sediment transport direction (Figure 7), similar to sand and silt deposits from running water in laboratory experiments [*Rees and Woodall*, 1975]. In lacustrine sediments, the oblate AMS ellipsoid lies on the depositional plane with some possible superimposed anisotropy, and the elongated grains roll on the bedding plane due to gravity [*Tarling and Hrouda*, 1993]. This possibility is the least for

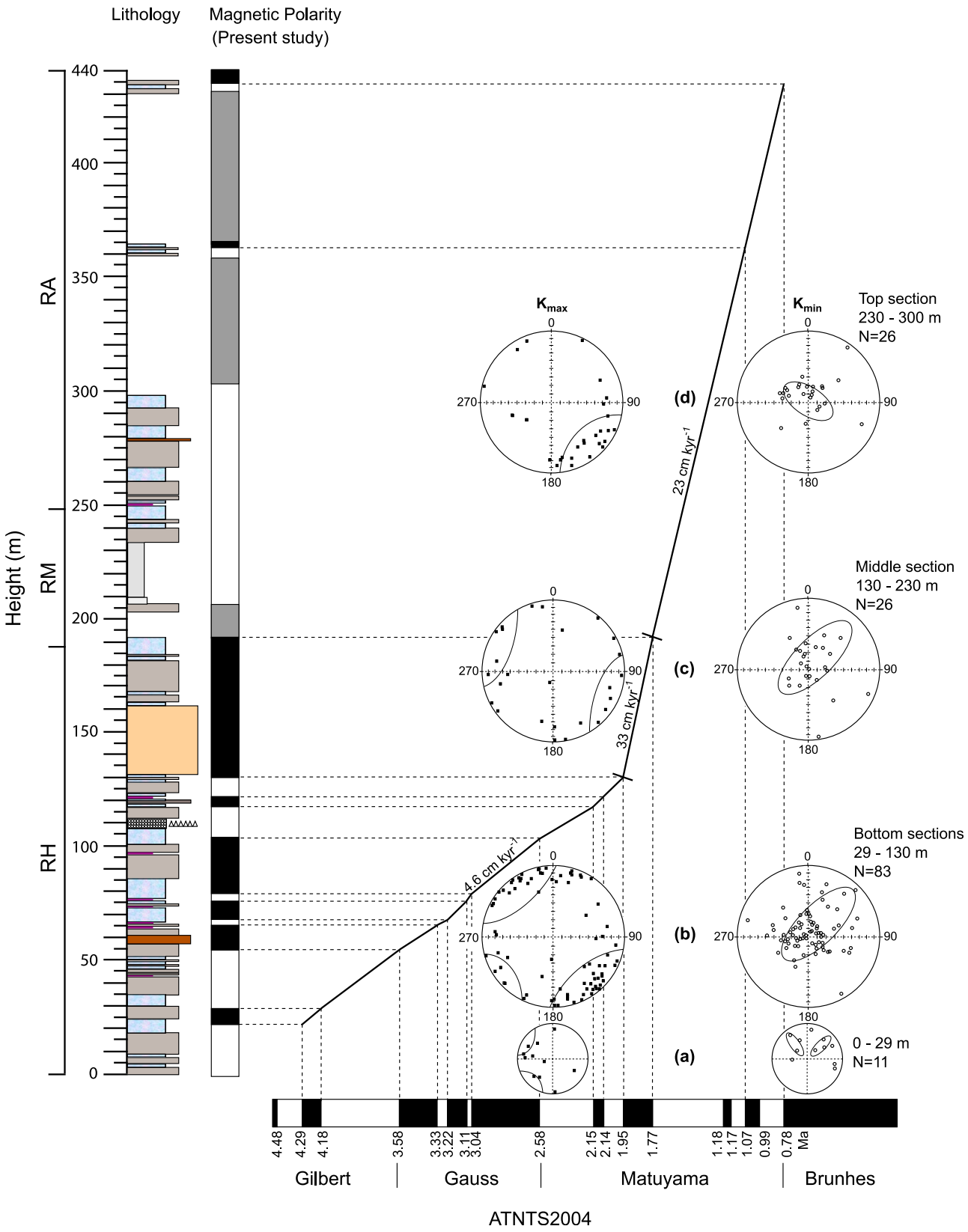

Figure 7. Chronostratigraphic correlation between MPS and ATNTS2004 and evaluated sediment accumulation rates. Equal area projections (lower hemisphere) of the directions of K_{max} (solid squares) and K_{min} axes (open circles) of AMS ellipsoids subdivided for the samples from bottom: (0–130 m): (a) 0–29 m, and (b) 30–130 m; middle: (c) 130–230 m; and top: (d) 230–300 m. The orientation of K_{max} and K_{min} axes is qualitatively indicated in the stereograms.

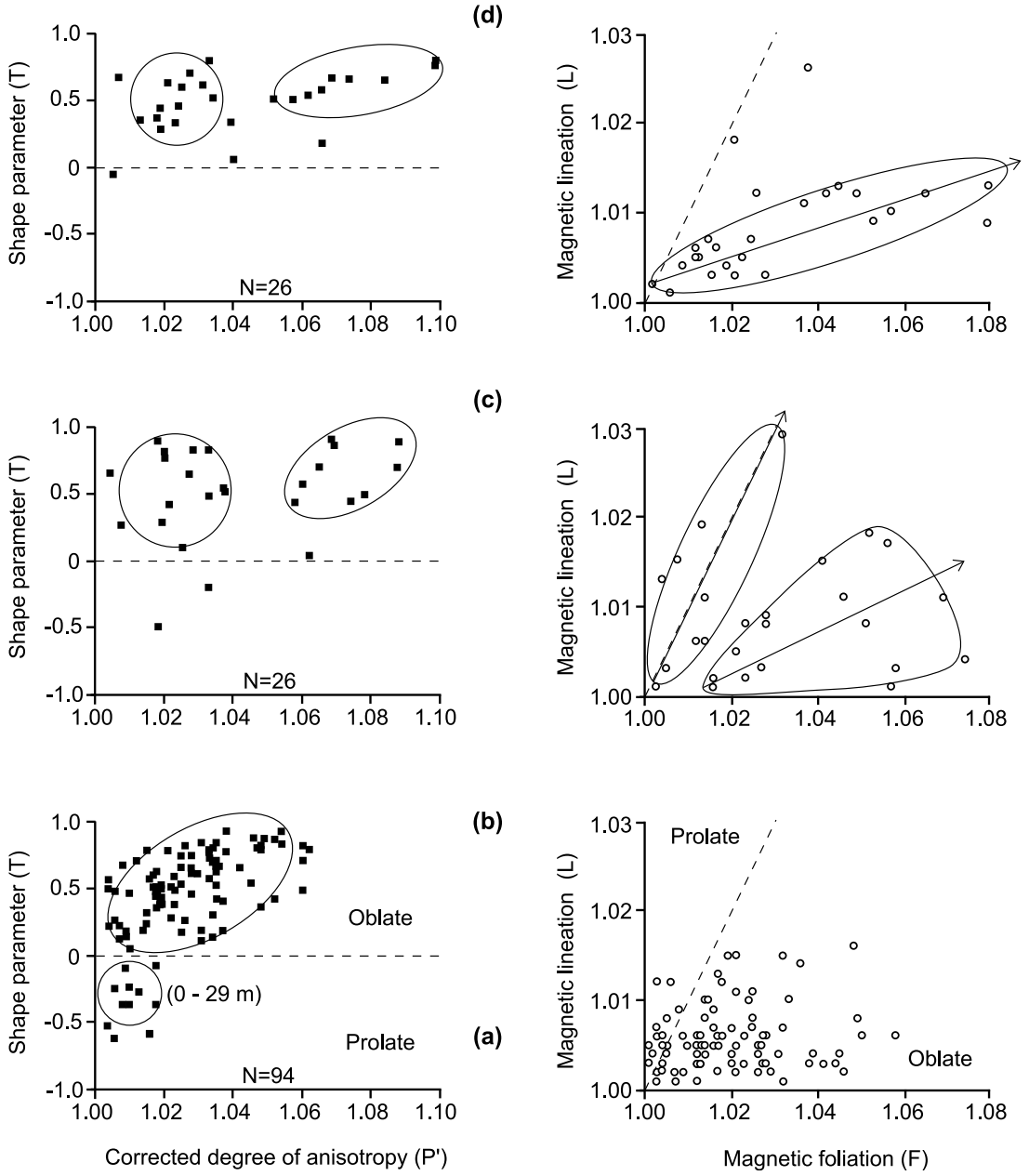

Figure 8. Plots of the corrected degree of anisotropy (P′) versus the shape parameter (T) (left) and degree of magnetic foliation (F) versus magnetic lineation (L) (right) showing a tendency to higher sediment accumulation rate (SAR) with higher P′. Samples from (a, b) bottom section (0–130 m): low SAR, (c) middle (130–230 m): highest SAR, and (d) top (230–300 m): relatively high SAR. The trend of data is qualitatively indicated in the diagrams.

our sequence, because K_{max} axes in the bottom and top parts of the succession show concentrations along the trends of the dispersion of K_{min} axes (Figures 7b, 7d), indicating direction of fluvial flow [*Tarling and Hrouda*, 1993]. Significant variation in tilts of K_{min} axes from near-vertical position (Figure 7), therefore, suggests that the Kashmir valley sediments, although mostly of the lacustrine type, have also witnessed fluvial activity (localized). This feeble fluvial activity did not modify the shape of AMS ellipsoids from the oblate to the prolate type (Figures 8c, 8d), and thus AMS data can be used to ascertain the paleocurrent direction. The increasing degree of anisotropy (P′) of the oblate ellipsoids revealed in our studied sequence also favors this conclusion.

[37] Our AMS data suggest that during the middle Gilbert chron (4.40 and 4.18 Ma) sedimentation was dominated by a NE- and NW-flowing fluvial regimes (Figure 7a). The orthogonal relationship between the long axes of K_{min} ellipsoid and respective clusters of K_{max} axes in this section suggests a strong flow velocity [cf. *Granar*, 1958]. In the remaining upper Gilbert, Gauss, and lower Matuyama chrons (4.18 to 1.95 Ma), the flow direction shifted toward the NE (Figure 7b). Scatter in the K_{min} axes suggests that deposition occurred on a low-gradient depositional plane.

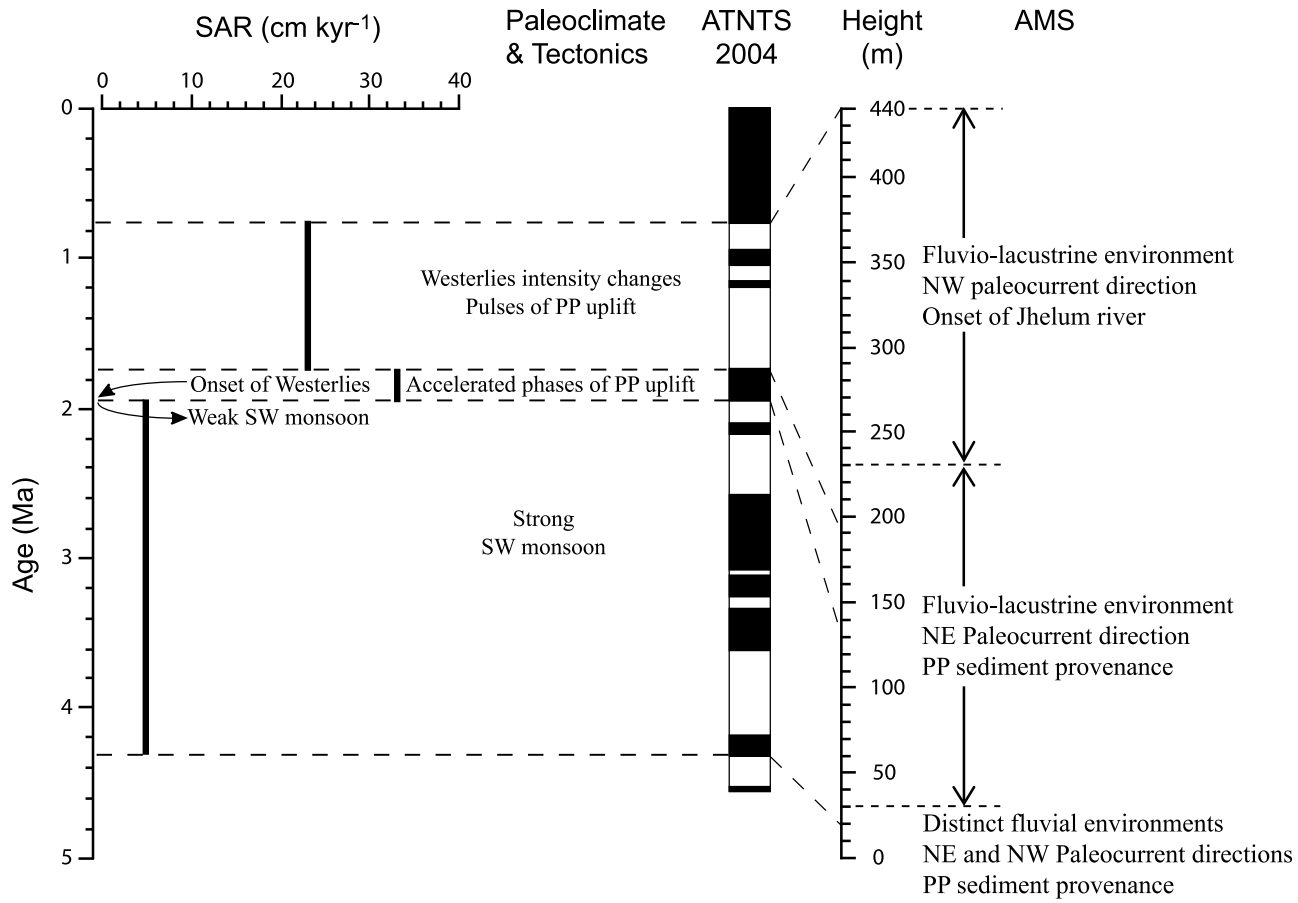

Figure 9. Sediment accumulation rate (SAR), paleoclimate tectonics, ATNTS2004 and AMS characteristics of Karewa Lake sediment of the Romushi river section in the period from 4.40 to 0.77 Ma. PP, Pir Panjal.

This observation is in accordance with the results reported by *Burbank and Johnson* [1983] suggesting that the Pir Panjal at the SW was the major source of sediment into the ambient lake. The sudden change of the AMS ellipsoid shape from prolate to oblate type in the succeeding section indicates a drastic change of fluvial environment in the Kashmir valley from fluvial to lacustrine type at 4.18 Ma (Figures 8a, 8b). The broadly increasing linear distribution of most of the data in the oblate field for the section between ~29 and 130 m (upper Gilbert, Gauss, and lower Matuyama chrons) probably indicates a progressive increase in energy of the fluvial system during deposition of these dominantly lacustrine sediments, thereby causing an increasing degree of anisotropy of the AMS ellipsoid. The clusters of K_{max} axes show both parallel and orthogonal concentrations with reference to the long axis of the K_{min} ellipsoid (Figure 7b). When comparing these results with theories and experiments [*King*, 1955; *Granar*, 1958; *Ellwood*, personal communication, in *Tarling and Hrouda*, 1993], our data indicate wide fluctuations of fluvial velocities during deposition.

[38] Our results from the sedimentary sequence between 130 and 230 m (middle Matuyama chron) (Figure 7c) show that the provenance was in the south (Pir Panjal). Nearly orthogonal relationship, between the long axis of K_{min} ellipsoid and the K_{max} clusters for this section, suggests stronger episodic fluvial flow within dominantly lacustrine environment. In the P′ versus T plots (Figure 8c), there are two distinct clusters in the oblate field, indicating two distinct fluvial systems of relatively low and high energy, respectively, within a dominant lacustrine environment present at that time. This is also demonstrated by AMS data (Figure 8d). During the upper Matuyama and the Brunhes chrons, the direction of the fluvial flow changed by 90° toward the NW and mirrors the present flow direction of the Jhelum river. Our observations are at variance with the suggestion made by *Burbank and Johnson* [1983], who suggested the emergence of the Jhelum river to ~2.4 Ma, whereas our data indicate that it came into being ~1.07 Ma. The fluvial velocity during this period appears to have receded when compared with theories and experiments [*King*, 1955; *Granar*, 1958; *Ellwood*, personal communication, in *Tarling and Hrouda*, 1993].

5.3. Sedimentation and Tectonics

[39] It has been established that the thick conglomeratic horizon occurring at the base of the Karewa Group was deposited during high-energy stream flow in contrast to the succeeding fluviolacustrine members of this sequence [*Burbank and Johnson*, 1983]. The base of the lacustrine sediments overlying the Pir Panjal Trap in the lower Karewa Group has been established to be ~4.05 Ma [*Burbank and Johnson*, 1982]. The top of this sequence, marking the

onset of the 200- to 300-m-thick conglomerate, is thought to be close to ~3.15 Ma, and the top of the conglomerate sequence older than 3.05 Ma [*Agrawal et al.*, 1989]. On the basis of this chronology, the SARs of the basal lacustrine sediments and the overlying conglomeratic horizon are recalculated to be ~28 cm kyr^{-1} and >300 cm kyr^{-1}, respectively. The rest of the Gauss and whole Matuyama chron has estimated sedimentation rates of ~68 and ~22 cm kyr^{-1} respectively, if the thin conglomerate horizons present within these sequences are discounted.

[40] Visual comparison of the ATNTS2004 polarity chrons of *Lourens et al.* [2004] and magnetostratigraphy data of our studied sequence (Figure 7) shows that the SAR varies from as low as ~4.6 cm kyr^{-1} in the bottom section (up to 130 m height) of the succession to a high value of ~33 cm kyr^{-1} in the middle section (130 to 190 m). A relatively low SAR of ~23 cm kyr^{-1} is calculated for the top section of the sequence (>190 m). Our SAR data suggest that the deposition of lacustrine sediment with low SAR (4.6 cm kyr^{-1}) prevailed until ~1.95 Ma at Romushi. However, there was a sudden increase in the SAR to ~33 cm kyr^{-1} between 1.99 and 1.77 Ma. At the top of the section (<1.77 Ma), the same history continued with a possibility of reduced intensity, resulting in a decreased SAR to ~23 cm kyr^{-1}. Our findings of high SAR values of ~33 cm kyr^{-1} are consistent with the history of evolution of Kashmir valley coinciding with the uplift of lower Karewas during the most recent Himalayan orogenic movements [*Balasubrahmanyan*, 2006].

5.4. Climatic Implications

[41] Currently, the Kashmir intermontane basin is dominated by a Mediterranean climate. However, in the beginning of Karewa sedimentation until ~3.0 Ma, the pollen data suggest that the Kashmir valley was under the influence of SW summer monsoon due to the marginally uplifted Pir Panjal mountain range in the south [*Agrawal et al.*, 1989]. A low SAR (4.6 cm kyr^{-1}) between 4.40 and 1.95 Ma could be due to landscape stability (tectonic quiescence) and well-vegetated lake catchment preventing accelerated erosion and thus sedimentation in the Karewa Lake (Figure 9). Pollen data obtained from the lake sediment also suggest a warm and temperate climate until ~3.8 Ma in the Kashmir valley [*Agrawal et al.*, 1989].

[42] Following this, a sudden increase in SAR (33 cm kyr^{-1}) between 1.95 and 1.77 Ma was observed. Sedimentological and pollen data indicate that the Pir Panjal mountain was rapidly uplifting [*Burbank and Johnson*, 1982; *Agrawal et al.*, 1989]. A steady growth of the orographic barrier in the south began to appear, and the Kashmir valley was gradually deprived of the SW monsoon. This would mean that precipitation-driven erosion was associated with winter monsoon. We suggest that all-time high SAR in the Karewa Lake could be due to an accelerated uplift of the southerly Pir Panjal ranges aided by westerlies, because sediment transport capacity is a function of stream power, which in turn is dictated by the discharge and gradient.

[43] Evidence of a first cold, temperate, and dry phase ~3.4 Ma is indicated by the first appearance of *arvicolid* (cold-loving rodent) [*Agrawal et al.*, 1989]. Because stream discharge deceases during cold climate, under such conditions, increased sediment flux can only take place if the stream gradient steepens enough to facilitate erosion during rainy events. In view of this, we attribute the enhanced SAR to an accelerated uplift of the Pir Panjal ranges. A similar observation was made by *Burbank and Johnson* [1982] for a near-identical SAR, which they also attributed to the source area uplift. Pollen data from Karewa sequence indicate a transition from a subtropical type of climate to a cool, temperate type with some variation in precipitation ~2.2 Ma. In the Siwalik sequence of Haripur Khol, the above period was represented by marshy conditions [*Phadtare et al.*, 1994]. Toward the top (between 1.77 and <0.77 Ma), a relative decrease in SAR (23 cm kyr^{-1}) was observed. We attribute this to marginal improvement in the rainfall condition particularly associated with westerlies (winter monsoon). Outside Kashmir basin, Siwalik sediments suggest a cool and dry climate [*Phadtare et al.*, 1994]. This is reasonable because the Siwaliks are located south of the Pir Panjal and are influenced by the SW summer monsoon.

6. Conclusions

[44] Our conclusions are as follows:

[45] 1. The 440-m-thick Romushi river section identifies the Pliocene-Pleistocene magnetostratigraphic sequence for the sediments of the Karewa Group, Kashmir basin, India. In all, eight normal and eight reversed polarity magnetozones have been identified from these sequences ranging in age from 4.40 to 0.77 Ma. The data, for the first time, provide a complete magnetostratigraphic framework of the basin fill within one section.

[46] 2. Our anisotropy of magnetic susceptibility data indicates that the sedimentation history of the Kashmir valley was dominated by a fluvial environment before 4.18 Ma with two dominant flow directions toward the NE and NW. This indicates that the Pir Panjal ranges at the SW were the major source of these sediments. The sedimentary sequence between upper Gilbert, Gauss, and lower Matuyama chron (~4.18 to 1.95 Ma) was found to be mostly of the fluviolacustrine type.

[47] 3. During the upper Gilbert, Gauss, and lower Matuyama chrons (~4.18 to 1.95 Ma), the restricted fluvial direction within the dominant lacustrine environment was mostly toward the NE, indicating that the Pir Panjal ranges remained the major source of these sediments.

[48] 4. From the middle Matuyama (~1.95 to 1.07 Ma) onward, the direction of fluvial flow remained toward the NE with a relatively strong fluvial velocity. In the upper Matuyama and lower Brunhes chron (~1.07 to 0.77 Ma), there was a change in the fluvial velocity, and it was directed toward the NW, which indicates the onset of the ancestral Jhelum river flow in the basin.

[49] 5. The calculated sediment accumulation rates (SAR) for the whole Karewa Group are found to vary from 4.6 cm kyr^{-1} during the upper Gilbert (~4.29–3.58 Ma), the entire Gauss (3.58–2.58 Ma), and early Matuyama (2.58–1.95 Ma) chrons to 33 cm kyr^{-1} during the Olduvai subchron in the middle to late Matuyama (1.95–1.77 Ma) chron. An SAR of 23 cm kyr^{-1} was estimated for the middle to late Matuyama and early Brunhes chrons.

[50] 6. Climatically, the valley was under the influence of the SW monsoon till ~1.95 Ma. After this period, an accelerated uplift of the Pir Panjal ranges prevented the SW

monsoon from entering into the Kashmir valley. Since then, the changing intensities of the westerlies coupled with the pulsating uplift along the southern flank (Pir Panjals) caused the spatial and temporal changes in Karewa sedimentation until ~0.77 Ma.

[51] **Acknowledgments.** We are thankful to S. K. G. Krishnamacharyulu, R. K. Pant, Habib Alimohammadian, J. N. Prasad, P. R. Chauhan, and S. Kusumgar for offering their valuable suggestions and comments. NB and EA are thankful to DFG, Germany, for supporting the HIMLAKES project [AP 34/15]. BVL is thankful to CSIR, Delhi, for sponsoring the fellowship to pursue the research work. The quality of the manuscript has been greatly improved on the basis of suggestions and comments of Brooks Ellwood, Cor Langereis, and an anonymous reviewer. We thank the editor and associate editor for providing encouragement and support.

References

Agarwal, K. K., and G. K. Agrawal (2005), A genetic model of thrust-bounded intermontane basin using scaled sandbox analogue models: an example from the Karewa Basin, Kashmir Himalayas, India, *Int. J. Earth Sci.*, *94*(1), 47–52.

Agrawal, D. P. (1985), Cenozoic climatic changes in Kashmir: the multidisciplinary data, in *Climate and Geology of Kashmir and Central Asia: The Last 4 Million Years*, edited by D. P. Agrawal et al., pp. 1–12, Today and Tomorrow's Printers, New Delhi, India.

Agrawal, D. P. (1988), Palaeoclimatic data from Kashmir: a synthesis and some correlations, *Proc. Indian Nat. Sci. Acad.*, *54A*(3), 333–344.

Agrawal, D. P., R. Dodia, B. S. Kotlia, H. Razdan, and A. Sahni (1989), The Plio-Pleistocene geologic and climatic record of the Kashmir valley, India: a review and new data, *Palaeogeogr., Palaeoclimatol., Palaeoecol.*, *73*, 267–286.

Agrawal, D. P., S. Kusumgar, and R. V. Krishnamurthy (Eds.) (1985), *Climate and Geology of Kashmir and Central Asia: The Last 4 Million Years*, Today and Tomorrow's Printers, New Delhi, pp. 1–247.

Appel, E., and H. C. Soffel (1985), Domain state of Ti-rich titanomagnetites deduced from domain structure observations and susceptibility measurements, *J. Geophys. Res.*, *56*, 121–132.

Badam, G. L. (1972), Additional mammalian fossils in the Karewas of Kashmir, *Curr. Sci.*, *41*(1), 529–530.

Balasubrahmanyan, M. N. (2006), *Geology and Tectonics of India: An Overview*, Memoir No. 9, International Association for Gondwana Research, Kochi, Japan.

Bhatia, S. B. (1968), Pleistocene ostracods from the upper Karewa of Kashmir, India, *Micropalaeontology*, *14*(4), 465–483.

Bhatia, S. B., S. R. Batra, and B. S. Kotlia (1985), Ostracodes and palaeoecology of the Karewa Formation of Hirpur and Romushi sections, Kashmir, India, in *Climate and Geology of Kashmir and Central Asia: The Last 4 Million Years*, edited by D. P. Agrawal et al., pp. 45–52, Today and Tomorrow's Printers, New Delhi.

Bhatt, D. K. (1975), On the Quaternary geology of Kashmir Valley with special reference to stratigraphy and sedimentation, *Geol. Surv. India Misc. Pub.*, *24*(1), 188–203.

Bhatt, D. K. (1976), Stratigraphical status of the Karewa group of Kashmir, India, *Himalayan Geol.*, *6*, 197–208.

Bhatt, D. K. (1989), Lithostratigraphy of Karewa Group, Kashmir Valley, India and a critical review of its fossil record, *Geol. Surv. India Memoirs*, *122*, pp.15–38.

Bhatt, D. K., and A. K. Chatterji (1976), An appraisal of field observations on the geology of the Plio-Pleistocene Karewa Group and more recent Quaternary deposits of Kashmir Valley, *Proc. VI Indian Colloq. Micropaleontol. Stratigr.*, pp. 11–21.

Burbank, D. W. (1985), The age of the Karewas, Kashmir as determined from fission-track dating and magnetostratigraphies, in *Climate and Geology of Kashmir and Central Asia: The Last 4 Million Years*, edited by D. P. Agrawal et al., pp. 19–26, Today and Tomorrow's Printers, New Delhi.

Burbank, D. W., and G. D. Johnson (1982), Intermontane-basin development in the past 4 Myr in the north-west Himalaya, *Nature*, *298*, 432–436.

Burbank, D. W., and G. D. Johnson (1983), The Late Cenozoic chronologic and stratigraphic development of the Kashmir intermontane basin, northwestern Himalaya, *Palaeogeogr., Palaeoclimatol., Palaeoecol.*, *43*, 205–235.

De Terra, H., and T. T. Paterson (1939), Studies on the Ice age in India and the associated human cultures, *Carnegie Inst. Wash. Publ.*, *493*, 1–354.

Garćes, M., W. Krijgsman, J. Van Dam, J. P. Calvo, L. Alcalá, and A. M. Alonso-Zarza (1997), Late Miocene alluvial sediments from the Teruel area: Magnetostratigraphy, magnetic susceptibility, and facies organization, *Acta Geologica Hispanica*, *32*, 171–184.

Gautam, P., and W. Rösler (1999), Depositional chronology and fabric of Siwalik group sediments in Central Nepal from magnetostratigraphy and magnetic anisotropy, *J. Asian Earth Sci.*, *17*, 659–682.

Gautam, P., A. Hosoi1, K. R. Regmi, D. R. Khadka, and Y. Fujiwara (2000), Magnetic minerals and magnetic properties of the Siwalik Group sediments of the Karnali river section in Nepal, *Earth Planet. Space*, *52*, 337–345.

Granar, L. (1958), Magnetic measurements on Swedish varved sediments, *Arkive fur Geofysik*, *3*, 1–40.

Hamilton, N., and A. I. Rees (1970), The use of magnetic fabric in paleocurrent estimation, pp. 445–464, in *Palaeogeophysics*, edited by S. K. Runcorn, Academic Press, London.

Hrouda, F. (2007), Magnetic susceptibility, anisotropy, in *Encyclopedia of geomagnetism and paleomagnetism*, edited by David Gubbins and Emilio Herrero-Bervera, pp. 546–560, Springer, Netherlands.

Johnson, G. D., P. Zeitler, C. W. Naeser, N. M. Johnson, D. M. Summer, C. D. Frost, N. D. Opdyke, and R. A. K. Tahirkheli (1982), The occurrence and Fission-track ages of Late Neogene and Quaternary volcanic sediments, Siwalik Group, northern Pakistan, *Palaeogeogr., Palaeoclimatol., Palaeoecol.*, *37*, 63–93.

King, R. F. (1955), The remanent magnetism of artificially deposited sediments, *Mon. Not. R. Astr. Soc.*, *7*, 115–134.

Kirschvink, J. L. (1980), The least-squares line and plane and the analysis of palaeomagnetic data, *Geophys. J. R. Astr. Soc.*, *62*, 699–718.

Kodama, K. P., E. B. Evenson, J. M. Clinch, and J. Rabassa (1985), Anomalous geomagnetic field behavior recorded by glacial sediments from northwestern Patagonia, Argentina, *J. Geomag. Geoelect.*, *37*, 1035–1050.

Kusumgar, S., N. Bhandari, and D. P. Agrawal (1985), Fission track ages of the Romushi lower Karewas, Kashmir, in *Climate and Geology of Kashmir and Central Asia: The Last 4 Million Years*, edited by D. P. Agrawal et al., pp. 245–247, Today and Tomorrow's Printers, New Delhi.

Lourens, L. J., F. Hilgen, N. J. Shackleton, J. Laskar, and D. Wilson (2004), The Neogene period, in *A Geologic Time Scale 2004*, edited by F. M. Gradstein, J. G. Ogg, and A. G. Smith, pp. 409–440, Cambridge University Press, Cambridge.

McFadden, P. L., and M. W. McElhinny (1990), Classification of the reversals test in paleomagentism, *Geophys. J. Int.*, *103*, 725–729.

Ori, G. G., and P. F. Friend (1984), Sedimentary basins formed and carried piggyback on active thrust sheets, *Geology*, *12*, 475–478.

Phadtare, N. R., R. Kumar, and P. K. Ghosh (1994). Stratigraphic palynology, floristic succession and the Tatrot/Pinjor boundary in upper Siwalik sediments of Haripur Khol area, district Sirmaur (HP), India, *Himalayan Geol.*, *15*, 69–82.

Rees, A. I., and W. A. Woodall (1975), The magnetic fabric of some laboratory deposited sands, *Earth Planet. Sci. Lett.*, *25*, 121–130.

Rehacek, J. (1994), *PMAGIC Software for Paleomagnetic Calculations*, *Version 1.2*, Department of Geology, Washington State University, Pullman.

Reynolds, R. L., J. G. Rosenbaum, P. Van Metre, M. Tuttle, E. Callender, and A. Goldin (1999), Greigite (Fe3S4) as an indicator of drought: The 1912-1994 sediment magnetic record from White Rock Lake, Dallas, Texas, USA, *J. Paleolim.*, *21*, 193–206.

Ricci-Lucchi, F. (1986), The Oligocene to recent foreland basins of the northern Apennines, in *Foreland Basins*, edited by P. A. Allen and P. Homewood, pp. 105–139, *Int. Assoc. Sedimentol. Spec. Publ.*, 8.

Ricci-Lucchi, F. (1987), Semi-allochthonous sedimentation in the Apenninic thrust belt, *Sediment Geol.*, *50*, 119–134.

Rosenbaum, J., R. Reynolds, J. Smoot, and R. Meyer (2000), Anisotropy of magnetic susceptibility as a tool for recognizing core deformation: reevaluation of the paleomagnetic record of Pleistocene sediments from drill hole OL-92, Owen Lake, California, *Earth Planet. Sci. Lett.*, *178*, 415–424.

Roy, D. K. (1975), Stratigraphy and paleontology of the Karewa Group of Kashmir, *Geol. Sur. India Misc. Publ.*, *24*(1), 204–221.

Sangode, S. J., R. Kumar, and S. K. Ghosh (2001), Application of magnetic fabric studies in an ancient fluvial sequence of NW Himalaya, *Curr. Sci.*, *81*(1), 66–71.

Singh, I. B. (1982), Sedimentation pattern in the Karewa Basin, Kashmir Valley, India, and its geological significance, *J. Paleontol. Soc. India*, *27*, 71–110.

Soto, R., J. C. Larrasoana, L. E. Arlegui, E. Beamud, B. Oliva-Urcia, and J. L. Simon (2009), Reliability of magnetic fabric of weakly deformed mudrocks as a palaeostress indicator in compressive settings, *J. Struct. Geol.*, *31*(5), 512–522.

Steidtmann, J. R., and J. G. Schmitt (1988), Provenances and dispersal of tectogenic sediments in thin-skinned, thrusted terrains, in *New Perspectives*

in Basin Analysis, edited by K. Kleinspehn and C. Paola, pp. 353–366, Springer, Berlin.

Tarling, D. H., and F. Hrouda (1993), *The Magnetic Anisotropy of Rocks*, Chapman and Hall Publishers, London, pp. 95–115.

Tewari, B. S., and R. K. Kachroo (1977), On the occurrence of Equus sivalensis from Karewas of Shupian, Kashmir Valley, *Recent Res. Geol.*, *3*, 468–477.

Van Velzen, A. J., and J. D. A. Zijderveld (1992), A method to study alterations of magnetic minerals during thermal demagnetization applied to a fine-grained marine marl (Trubi formation, Sicily), *Geophys. J. Int.*, *110*, 79–90.

Wadia, D. N. (1976), *Geology of India*, Tata-McGraw Hill, New Delhi, India.

Yang, X., S. Wang, G. Tog, and X. Jiang (2000), Vegetational and climatic responses to tectonic uplift in the Heqing basin of Yunnan Province during the past 1.0 Ma, *Acta Micropal. Sinica*, *17*(2), 207–217.

Yoshida, M., and Y. Igarashi (1984), Neogene to quaternary lacustrine sediments in the Kathmandu Valley, Nepal, *J. Nepal Geol. Soc.*, *4*, 73–100.

E. Appel, Institut für Geowissenschaften, Universität Tübingen, D-72076 Tübingen, Germany.

N. Basavaiah, K. Deenadayalan, B. V. Lakshmi, S. Misra, and K. V. V. Satyanarayana, Indian Institute of Geomagnetism, Kalamboli, New Panvel, Navi Mumbai 410 218, India. (bas@iigs.iigm.res.in)

N. Juyal, Physical Research Laboratory, Navrangpura, Ahmedabad 380 009, India.

M. A. Malik, University of Jammu, Jammu Tawi 180 006, India.